IIETA International Information and Engineering Technology Association
Advancing the World of Information and Engineering

Journal Européen des Systèmes Automatisés
Vol. 58, No. 1, January, 2025, pp. 31-38
Journal homepage: http://iieta.org/journals/jesa

Adaptive Sliding Mode Control for Maximum Power Point Tracking in Photovoltaic Systems

Anh Van Le, Linh Thi To Vu*

Faculty of Electricity and Automation, University of Economics – Technology for Industries, Hanoi 100000, Vietnam

Corresponding Author Email: vttlinh@uneti.edu.vn

https://doi.org/10.18280/jesa.580104

Received: 9 November 2024
Revised: 6 January 2025
Accepted: 20 January 2025
Available online: 31 January 2025

Keywords:
ASMC, MPPT, fuzzy controller, observer, P&O

ABSTRACT

Nowadays, photovoltaic (PV) systems are widely used in daily life and in many critical fields such as agriculture, industry, and exploration. Designing a controller to ensure that the PV system consistently achieves high efficiency during operation is always of interest to the scientific community. The PV system must maintain operation at the maximum power point tracking (MPPT) to optimize efficiency. Beyond the influence of intrinsic parameters like temperature and radiation, it is also significantly affected by external disturbances and variations in the power conversion circuit. Hence, an effective control strategy is required to mitigate these impacts. This paper introduces an adaptive sliding mode control (ASMC) approach for MPPT in PV systems. Initially, the Perturb & Observe (P&O) algorithm determines the reference voltage for the control scheme. Then, an adaptive sliding mode controller is designed to accurately track this reference while an observer estimates uncertainties and external disturbances. To further minimize chattering effects, a fuzzy controller is incorporated. The stability of the proposed controller is guaranteed based on the Lyapunov criterion, ensuring both adaptability and robustness. Finally, comparative simulations are conducted to validate its performance.

1. INTRODUCTION

Renewable energy has been playing an essential role in electricity production. Solar power is a widely accessible renewable energy source that is both eco-friendly and sustainable. It is a potential and popular choice in the fields of agriculture, industry, services, etc. [1-5]. The problem of improving PV systems' efficiency has attracted many scientists' attention [6-10]. The current-voltage (I-V) and power-voltage (P-V) characteristics of PV systems exhibit nonlinear behavior, varying dynamically with changes in radiation intensity and temperature. There is a single maximum point on these characteristics, which changes with different radiation and temperature values. The objective of the control strategy is to ensure that the PV system continuously operates at the maximum power point (MPP) to optimize energy extraction.

A DC/DC (Direct Current) converter is integrated with the PV system to regulate its output voltage. Common types of DC/DC converters include buck, boost, and buck-boost converters. Switching components such as MOSFETs and IGBTs (Insulated-Gate Bipolar Transistors) are employed to regulate the converters, with control pulses generated using pulse-width modulation (PWM). The controller's task is to create a pulse width for the PWM stage, in which the pulse width has a value from [0,1].

MPPT algorithms are developed in two forms, namely indirect algorithms and direct algorithms. The direct algorithm is commonly used because it only uses information about voltage and current. Meanwhile, in addition to requiring information about voltage and current, the indirect algorithm also involves information about temperature and radiation parameters as control parameters [3, 11]. Therefore, it is difficult for the indirect algorithm to perform well when radiation and temperature change. The P&O and Incremental Conductance (INC) methods are widely adopted direct approaches due to their simplicity and ease of implementation. However, a common drawback of these algorithms is their tendency to oscillate around the MPP under stable radiation conditions and their inability to effectively track the MPP during rapid radiation changes [2, 12-14]. On the other hand, the performance of the PV system is influenced by parameter uncertainties and external disturbances. In reference [15], a sliding mode controller was developed with a surface formulated based on the MPP. However, a major limitation of this approach is the chattering phenomenon occurring in the system. In reference [16], the authors introduced an MPPT controller utilizing quadratic sliding mode control, but the chattering issue persisted. On the contrary, in reference [17], a type 2 fuzzy and sliding mode-based MMPT controller was proposed, eliminating the chattering phenomenon. However, it did not consider the influence of uncertain parameters and external disturbances. Additionally, MPPT techniques utilizing fuzzy logic and neural networks [18, 19] have also been explored and implemented. However, these algorithms are more complex than the conventional MPPT, a simple and low-cost algorithm. The control strategies mentioned above are utilized to generate pulse width values for PWM, which

regulate the switching components of the DC/DC converter.

The control strategies mentioned above are utilized to generate pulse width values for PWM, which regulate the switching components of the DC/DC converter. To enhance control performance, MMPT techniques have been developed employing a two-loop control structure. In this structure, the first loop is responsible for setting the reference voltage, while the second loop adjusts the voltage tracking of the PV system based on the reference. For the first loop, widely used algorithms include P&O and INC. The effectiveness of the tracking process is heavily reliant on the tracking controller's performance in the second loop. The success of the tracking process is primarily determined by how well the controller functions in the second loop. A suitable control method should be capable of accurately tracking the MPP in various scenarios while handling the system's nonlinearities and uncertainties. In reference [20], the authors introduce an MPPT approach that integrates P&O with a sliding mode controller for photovoltaic applications, where the P&O method operates in the first loop and the sliding mode controller manages the reference voltage tracking in the second loop. However, this controller does not address the uncertain parameters, and the chattering phenomenon has not been eliminated. On the contrary, in reference [21], a control scheme based on P&O and sliding mode controller for PV systems was introduced to ensure robustness against the influence of disturbances and uncertainties of system parameters. However, the chattering phenomenon was not eliminated. In reference [22], the authors used the INC algorithm in the first loop and introduced the terminal sliding controller for the second loop. However, the algorithms [21, 22] did not eliminate the chattering phenomenon. In reference [23], the chattering phenomenon of the sliding controller was eliminated by automatic switching factor adjustment. However, it did not consider the uncertain parameters and external disturbances. In addition, in reference [24], an observer combined with the P&O method and a sliding controller was designed for PV systems. Unfortunately, it did not eliminate the chattering phenomenon.

From the analysis provided, this paper presents an adaptive sliding mode control (ASMC) approach to ensure the PV system consistently functions at the MPP. This is achieved using an observer and a fuzzy controller, where the observer estimates the uncertain components and unknown external disturbances, and the fuzzy controller adjusts the switching coefficient to reduce oscillations in the sliding mode control. The highlights and primary contributions of the paper are outlined below: (1) The ASMC employs a two-loop control scheme to enhance control quality, unlike the direct single-loop control schemes used in references [15-19]. (2) In contrast to references [20-24], the ASMC not only ensures the system consistently operates at the MPP but also eliminates the influence of external disturbances, uncertain parameters, and chattering phenomena.

2. MATHEMATICAL MODEL OF THE SYSTEM AND PROBLEM FORMULATION

2.1 Model of PV system

The PV system is modeled using either the one-diode equivalent circuit [25, 26] or the two-diode model [27, 28]. The mathematical representation of the PV array using the one-diode equivalent circuit model is expressed as follows [29]:

$$I_{pv} = N_P I_{ph} - N_P I_s \exp\left(\frac{V_{pv} + \beta R_s I_{pv}}{N_s \delta V_T} - 1\right) - \frac{V_{pv} + \beta R_s I_{pv}}{\beta R_p} \quad (1)$$

where, N_s represents the number of solar panels connected in series, N_p denotes the number of solar panels connected in parallel, I_{pv} and V_{pv} denote the output current and voltage of the PV array, respectively, the ideality factor appears as δ, $\beta = \frac{N_s}{N_p}$. By R_s has a minimal value, R_p has an immense value; Eq. (1) is rewritten as follows:

$$I_{pv} = N_P I_{ph} - N_P I_s \exp\left(\frac{V_{pv}}{N_s \delta V_T} - 1\right) \quad (2)$$

Using the mathematical models presented in Eq. (1) or Eq. (2) along with the electrical specifications of the PV module, the I-V and P-V curves under varying irradiance levels and a constant temperature are generated. To examine the I-V and P-V characteristics of the PV system, we consider a specific configuration using Sun Power SPR-305E-WHT-D PV modules, where 66 strings are connected in parallel, and each string consists of 5 PVs connected in series [17, 20]. The Sun Power SPR-305E-WHT-D PV module has the following specifications: a maximum power output of 305.226 W, an open-circuit voltage of 64.2 V, a short-circuit current of 5.96 A, a voltage of 54.7 V at the MPP, and a current of 5.58 A at the MPP. This PV system delivers 100 kW of maximum power under irradiance conditions of G=1000 W/m² and a temperature of T=25°C. Figure 1 displays the I-V and P-V curves of the system with varying irradiance conditions.

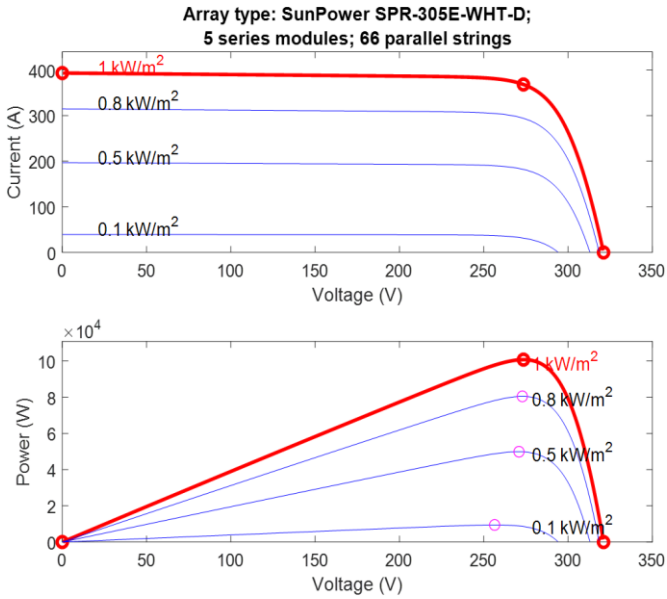

Figure 1. I-V and P-V characteristics of PV system [17, 20]

2.2 DC/DC boost converter

DC-DC converters are widely employed in photovoltaic power generation systems as an intermediary component connecting the photovoltaic panel and the load. In this paper,

we utilize a boost converter, with the circuit diagram shown in Figure 2, in which V_{pv} represents the input voltage, V_o stands for the output voltage, I_L refers to the induced current, R_o corresponds to the circuit load, u has a value in the range [0,1] is the pulse width of the PWM. The values of the circuit elements are selected in the manner outlined below [23]: L=0.005 H, C_v=5.10^{-3} F, C_o=5.10^{-3} F, R=4.9 Ω, the switching frequency of the PWM is selected as 5000 Hz.

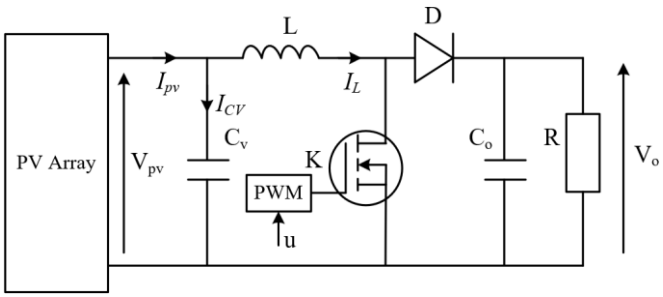

Figure 2. Boost converter circuit diagram

The dynamics of the boost converter is defined as follows [20]:

$$I_{CV} = (C_v + \bar{C}_v)\dot{V}_{pv} = I_{pv} - I_L \tag{3}$$

$$V_L = (L + \bar{L})\dot{I}_L = V_{pv} - V_o(1-u) \tag{4}$$

where, $\bar{C}_v$ and $\bar{L}$ are uncertain parameters, u is the control input with a value from [0,1]. From Eqs. (3) and (4), we get

$$\dot{V}_{pv} = -\frac{I_L}{C_v + \bar{C}_v} + \frac{I_{pv}}{C_v + \bar{C}_v} \tag{5}$$

$$\dot{I}_L = \frac{V_{pv}}{L + \bar{L}} - \frac{V_o}{L + \bar{L}} + \frac{V_o}{L + \bar{L}}u \tag{6}$$

Defining $\zeta = [V_{pv}, I_L]^T$, we get the following system of state equations:

$$\dot{\zeta} = f(\zeta) + \bar{f}(\zeta) + g(\zeta)u + d, \tag{7}$$

where,

$$f(\zeta) = \left[\frac{-I_L}{C_v + \bar{C}_v}, \frac{V_{pv}}{L + \bar{L}}\right]^T \text{ and } \bar{f}(\zeta) = \left[\frac{I_{pv}}{C_v + \bar{C}_v}, \frac{-V_o}{L + \bar{L}}\right]^T$$

represent the input nonlinear component.

$$g(\zeta) = \left[0, \frac{V_o}{L + \bar{L}}\right]^T$$

d is the unknown external disturbance.

Eq. (7) can be rewritten as

$$\dot{\zeta} = F(\zeta) + \bar{F}(\zeta) + G(\zeta)u + \psi(\zeta), \tag{8}$$

where,

$$F(\zeta) = \left[\frac{-I_L}{C_v}, \frac{V_{pv}}{L}\right]^T, \ \bar{F}(\zeta) = \left[\frac{I_{pv}}{C_v}, \frac{-V_o}{L}\right]^T,$$

$$G(\zeta) = \left[0, \frac{V_o}{L}\right]^T,$$

$$\psi(\zeta) = \Delta f(\zeta) + \Delta \bar{f}(\zeta) + \Delta g(\zeta) + d$$

2.3 Problem formulation

The goal is to design a controller that guarantees the system operates consistently at the MPP. First, the P&O method is used to determine the reference voltage V_{ref}. Then, the ASMC is designed to V_{pv} track V_{ref}, allowing the PV system to continuously operate at the MPP despite changes in irradiance and temperature. Figure 3 shows the layout of the controller, which includes a sliding mode controller, an observer, and a fuzzy controller. The observer estimates the uncertain components and external disturbances, while the fuzzy controller adjusts the coefficient in the sliding mode controller.

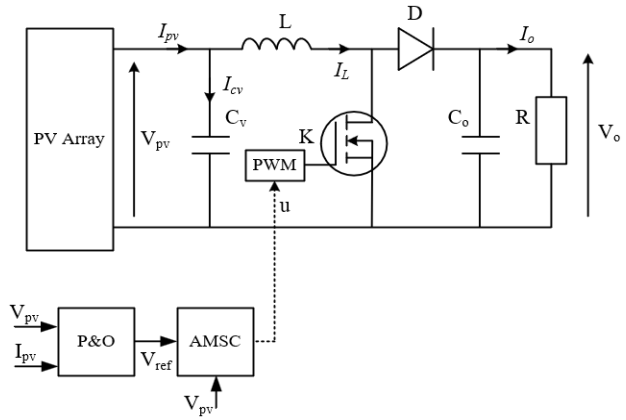

Figure 3. Control structure diagram

3. CONTROLLER DESIGN

3.1 P&O method

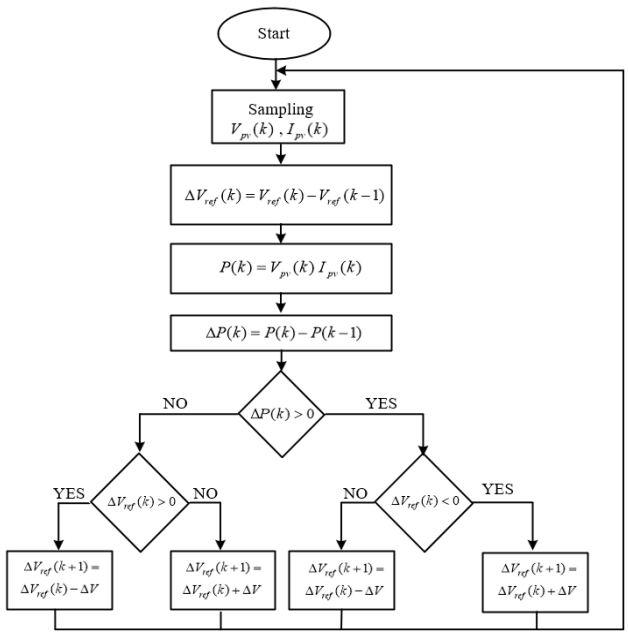

Figure 4. P&O method diagram

The P&O method is commonly applied to find the MPP of photovoltaic systems, owing to its straightforwardness and

effectiveness. It calculates a reference voltage V_{ref}, after measuring the output of the photovoltaic system. Figure 4 displays the sequence of steps for the P&O method [20], where ΔV_{ref} is a positive constant represents the increase or decrease of V_{ref} in each sampling period determined by comparing the power values from the current and previous sampling periods.

3.2 Adaptive sliding mode controller

3.2.1 Control law design

After determining V_{ref} through the P&O method, the ASMC control law is responsible for determining the control law for V_{pv} to track V_{ref}.

First, define tracking errors as follows: e_1=V_{pv}-V_{ref}, $e_2 = \dot{e}_1$, $e_2 = I_L - \dot{V}_{ref}$, $\dot{e}_2 = \dot{I}_L - \ddot{V}_{ref}$. The sliding surface is defined by the equation:

$$\bar{r} = \kappa_1 e_1 + e_2 \tag{9}$$

where, $\kappa_1 > 0$. By differentiating Eq. (9), we obtain:

$$\dot{\bar{r}} = \kappa_1 e_2 + \dot{e}_2 \tag{10}$$

Combining Eq. (8) and Eq. (10), we have

$$\dot{\bar{r}} = \kappa_1 e_2 + F(\zeta) + \bar{F}(\zeta) + G(\zeta)u + \psi(\zeta) - \ddot{V}_{ref} \tag{11}$$

By the target $\dot{\bar{r}} = 0$, we choose the control law as follows:

$$u = u_{td} + u_s \tag{12}$$

where, u_a is the component that pulls the states to the sliding surface defined as $u_a = G^{-1}(\zeta)\left(\ddot{V}_{ref} - F(\zeta) - \bar{F}(\zeta) - \kappa_1 e_2\right) - \hat{\psi}(\zeta)$, $\hat{\psi}(\zeta)$ is the estimate of $\psi(\zeta)$, u_s is the component that keeps the states on the sliding surface and moves towards the origin chosen as $u_s = -G^{-1}(\zeta)\kappa_2\, sgn(\bar{r})$, with $\kappa_2 > 0$ being the switching coefficient. The stability of the system with control law (12) is proven in the following section. The updated law of the observer is defined as

$$\dot{\hat{\psi}}(\zeta) = -\xi\bar{r} \tag{13}$$

where, ξ is a positive constant. The approximation error is defined as $\tilde{\psi}(\zeta) = \psi(\zeta) - \hat{\psi}(\zeta)$.

In the control law (12), if κ_2 is large, the system will quickly move towards the sliding surface, but the chattering phenomenon will oscillate vigorously, and vice versa. Therefore, κ_2 is selected by the fuzzy controller to reduce the chattering phenomenon.

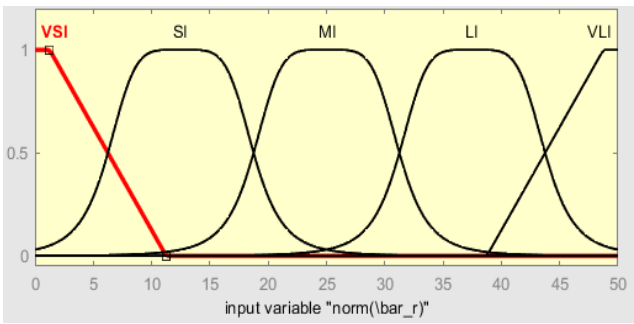

(a) Fuzzy function for input

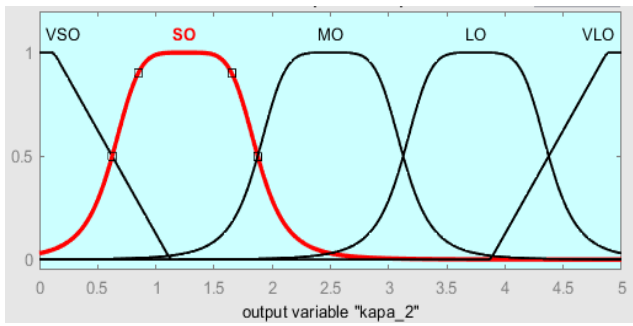

(b) Fuzzy function for output

Figure 5. Fuzzy functions for input and output

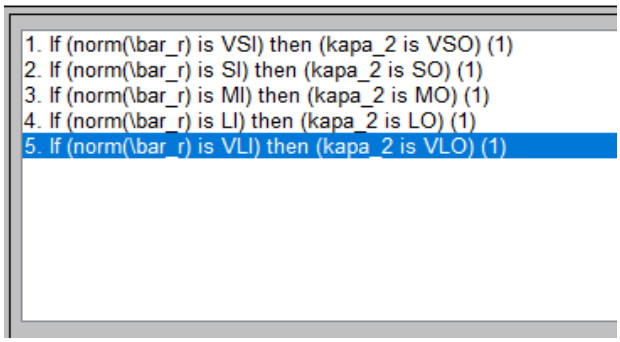

Figure 6. Control laws

The controller is designed with a single input and output structure, where the input is the sliding surface and the output is the coefficient κ_2. Figure 5 presents the fuzzy function for input and output, and Figure 6 depicts the control law. The MAX-MIN composition law is applied, and defuzzification is performed using the centroid method.

3.2.2 Proof of stability

The Lyapunov function is chosen as follows:

$$L = \frac{1}{2}\bar{r}^2 + \frac{1}{2}\xi\tilde{\psi}^2 \tag{14}$$

Taking the derivative Eq. (14) along the trajectory of Eq. (8), we get

$$\begin{aligned} \dot{L} &= \bar{r}\,\dot{\bar{r}} + \frac{1}{\xi}\tilde{\psi}\dot{\tilde{\psi}} \\ &= \bar{r}\left(\kappa_1 e_2 + F + \bar{F} + Gu + \psi - \ddot{V}_{ref}\right) + \frac{1}{\xi}\tilde{\psi}\dot{\tilde{\psi}} \end{aligned} \tag{15}$$

Substituting control law Eq. (12) into Eq. (15) one can obtain:

$$\dot{L} = \bar{r}\left(-\kappa_2\,\mathrm{sgn}(\bar{r}) + \left(\psi - \hat{\psi}\right)\right) + \frac{1}{\xi}\tilde{\psi}\dot{\tilde{\psi}} \tag{16}$$

$$= -\kappa_2 |\bar{r}| + \tilde{\psi}\bar{r} + \frac{1}{\xi}\tilde{\psi}\dot{\tilde{\psi}}$$

Replace updated law Eq. (13) into Eq. (16) one can obtain:

$$\dot{L} = -\kappa_2 |\bar{r}| \tag{17}$$

It can be seen that $\dot{L} \leq 0$ when $\kappa_2 > 0$. Therefore, the closed-loop system is stable according to the Lyapunov criterion. It is easy to see that, $L, \bar{r}, \dot{\bar{r}}, \int_0^t \dot{L}\, dt = -\kappa_2 \int_0^t |\bar{r}|\, dt$ are all limited. Apply Barbalat Lemma [30], when $t \to \infty$, we have $\bar{r} \to 0$, then $e_1 \to 0$, $\dot{e}_1 \to 0$.

4. RESULTS

In this section, the ASMC is applied to the Sun Power SPR-305E-WHT-D PV system. The simulation is performed on Matlab/Simulink 2021b software with the Specialized Power Systems toolbox.

The system simulation time is 3 seconds with the temperature kept constant at 25°C, the radiation has a value of 1000 W/m^2 from time 0 to 1.5 seconds and 500W/m^2 from time 1.5 to 3 seconds, $\bar{C}_v$ has a random value in the range $[-5.10^{-3}, 5.10^{-3}]F$, $\bar{L}$ has a random value in the range $[-0.01, 0.01]$mH. The controller parameters are chosen as follows: $\kappa_1 = 10$, the update coefficient of the observer $\xi = 0.5$. The P&O algorithm is performed with ΔV_{ref}=0.01V.

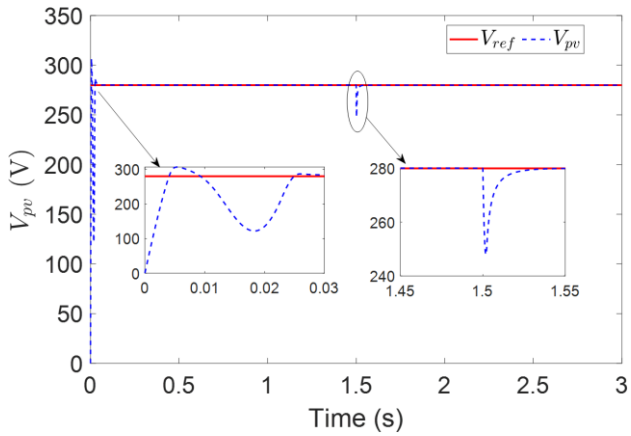

Figure 7. Reference voltage tracking

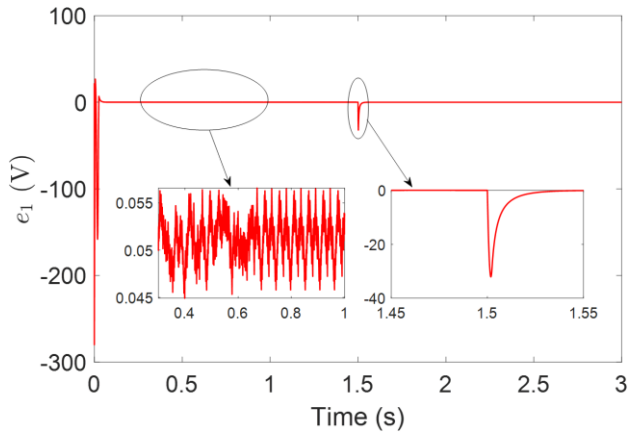

Figure 8. Reference voltage tracking error

The tracking results of the reference voltage and tracking error of ASMC are shown in Figure 7 and Figure 8. The results show that ASMC provides good tracking quality, with the response time for V_{pv} to reach the reference voltage being 0.025 milliseconds (see first subfigure of Figure 7) and the tracking error being within the range of [0.04,0.06]V (see first subfigure of Figure 8). At 1.5 seconds, the radiation is halved, and the tracking error increases but quickly returns to equilibrium (see second subfigure of Figure 7 and Figure 8). Accordingly, the system's voltage, current, and power under ASMC are presented in Figures 9-11. They show that the system always operates at MPP, with a response time of 0.2 seconds (see first subfigure of Figure 11).

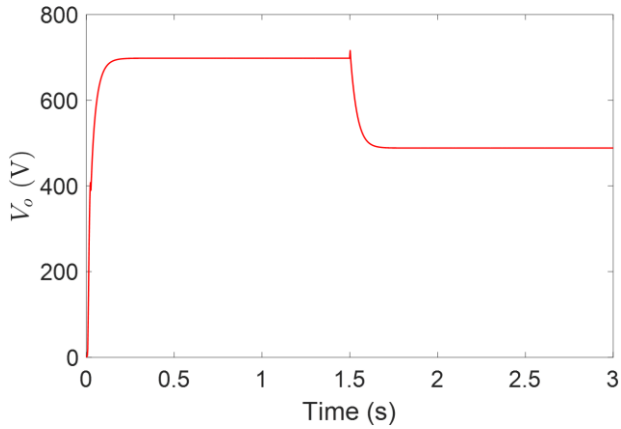

Figure 9. System output voltage

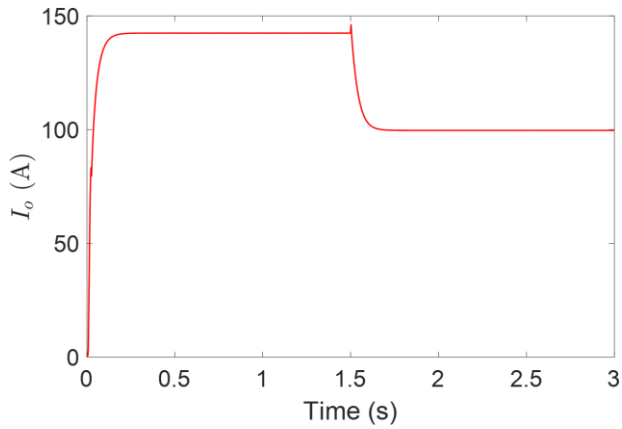

Figure 10. System output current

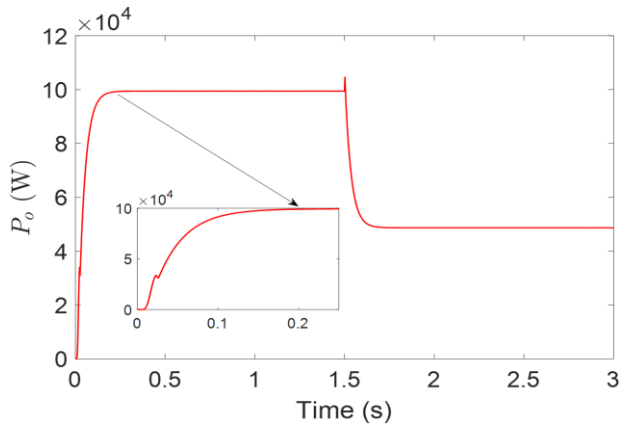

Figure 11. System output power

To assess the performance of the ASMC, comparative simulations were performed with the sliding mode controller (SMC) proposed in reference [20]. Since the controller does not address uncertain parameters, the simulations were conducted with constant system parameters to ensure a fair comparison [20]. Figure 12 displays a comparison of the output power between the controllers. It can be observed that the SMC causes considerable fluctuations around the maximum power point (chattering phenomenon), while the ASMC significantly reduces this chattering. Consequently, the ASMC demonstrates superior control quality compared to the SMC. Additionally, the ASMC ensures robustness against uncertain parameters. Therefore, the effectiveness of the ASMC was confirmed through simulation results.

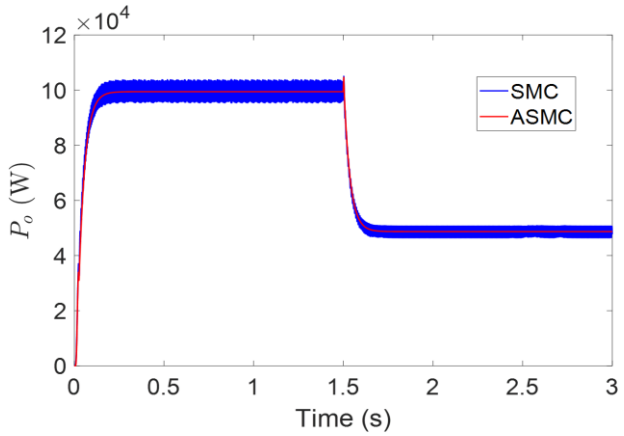

Figure 12. Compare the output power of ASMC and SMC

The simulation results show that ASMC provides good control performance, not only ensuring the system always operates at MPP but also ensuring sustainability and significantly reducing chattering. It can be seen that ASMC is a more comprehensive solution than references [15-24]. However, ASMC has only been verified through simulation. In future work, the proposed controller will be implemented on the STM32F1 microcontroller, and experiments will be conducted using the system structure diagram shown in Figure 3, in which the values of the boost converter circuit have been introduced in Section 2.2. On the other hand, the ASMC requires measurements of both voltage and current from the PV system. Therefore, ASMC needs to be developed to minimize the measurement sensors.

5. CONCLUSIONS

This paper has introduced an ASMC scheme for MMPT in PV systems. The proposed controller consists of a P&O method for generating the reference voltage, an adaptive sliding mode approach to ensure the system tracks the reference voltage, with an observer designed to estimate uncertain components and external disturbances, and a fuzzy controller to reduce the chattering phenomenon. The results of the simulation indicate that the ASMC effectively maintains operation at the MPP, not only ensuring the system always operates at MPP but also ensuring sustainability and significantly reducing chattering. It can be seen that ASMC is a comprehensive solution. However, ASMC has only been verified through simulation and requires both PV voltage and current sensors. In future work, we will test and develop the controller to minimize the measurement sensors.

ACKNOWLEDGMENT

This research was supported by the University of Economics - Technology for Industries (UNETI), Hanoi, Vietnam.

REFERENCES

[1] Parida, B., Iniyan, S., Goic, R. (2011). A review of solar photovoltaic technologies. Renewable and Sustainable Energy Reviews, 15(3): 1625-1636. https://doi.org/10.1016/j.rser.2010.11.032

[2] Esram, T., Chapman, P.L. (2007). Comparison of photovoltaic array maximum power point tracking techniques. IEEE Transactions on Energy Conversion, 22(2): 439-449. https://doi.org/10.1109/TEC.2006.874230

[3] Salas, V., Olías, E., Barrado, A., Lazaro, A. (2006). Review of the maximum power point tracking algorithms for stand-alone photovoltaic systems. Solar Energy Materials and Solar Cells, 90(11): 1555-1578. https://doi.org/10.1016/j.solmat.2005.10.023

[4] Schirone, L., Granello, P., Massaioli, S., Ferrara, M., Pellitteri, F. (2024). An approach for maximum power point tracking in satellite photovoltaic arrays. In 2024 International Symposium on Power Electronics, Electrical Drives, Automation and Motion (SPEEDAM), Napoli, Italy, pp. 788-793. https://doi.org/10.1109/SPEEDAM61530.2024.10609086

[5] Saxena, A., Kumar, R., Sagade, A.A., Singh, D.B., Tyagi, V.V., Cuce, E., Goel, V. (2024). A state-of-art review on photovoltaic systems: Design, performance, and progress. Process Safety and Environmental Protection, 190: 1324-1354. https://doi.org/10.1016/j.psep.2024.07.111

[6] Baviskar, S., Patil, G.B., Beldar, R. (2024). Predictive analysis of 50 kW solar photovoltaic system using PVSYST. In 2024 International Conference on Intelligent and Innovative Technologies in Computing, Electrical and Electronics (IITCEE), Bangalore, India, pp. 1-4. https://doi.org/10.1109/IITCEE59897.2024.10467946

[7] Ahmad, W., Qureshi, M.B., Khan, M.M., Fayyaz, M.A., Nawaz, R. (2023). Optimizing large-scale PV systems with machine learning: A neuro-fuzzy MPPT control for PSCs with uncertainties. Electronics, 12(7): 1720. https://doi.org/10.3390/electronics12071720

[8] Rawdhan, A.Y., Ahmed, M.S. (2024). Exploiting PV system performance: A combined approach using MPPT, IoT, cleaning, cooling, and neural networks. International Journal of Electrical and Electronics Research, 12(4): 1120-1126. https://doi.org/10.37391/IJEER.120401

[9] Al-Sharo, Y.M., Al Smadi, K., Al Smadi, T. (2024). Optimization of stable energy PV systems using the Internet of Things (IoT). Tikrit Journal of Engineering Sciences, 31(1): 127-137. http://doi.org/10.25130/tjes.31.1.11

[10] Elbaksawi, O., Elminshawy, N.A., Diab, S., Eltamaly, A.M., Mahmoud, A., Elhadidy, H. (2024). Innovative metaheuristic algorithm with comparative analysis of

MPPT for 5.5 kW floating photovoltaic system. Process Safety and Environmental Protection, 185: 1072-1088. https://doi.org/10.1016/j.psep.2024.03.082
[11] Femia, N., Petrone, G., Spagnuolo, G., Vitelli, M. (2017). Power Electronics and Control Techniques for Maximum Energy Harvesting in Photovoltaic Systems. CRC Press.
[12] Hohm, D.P., Ropp, M.E. (2003). Comparative study of maximum power point tracking algorithms. Progress in Photovoltaics: Research and Applications, 11(1): 47-62. https://doi.org/10.1002/pip.459
[13] Sera, D., Mathe, L., Kerekes, T., Spataru, S.V., Teodorescu, R. (2013). On the perturb-and-observe and incremental conductance MPPT methods for PV systems. IEEE Journal of Photovoltaics, 3(3): 1070-1078. https://doi.org/10.1109/Jphotov.2013.2261118
[14] Issa, H.A., Mohammed, H.J., Abdali, L.M., Al Bairmani, A.G. (2021). Mathematical modeling and controller for PV system by using MPPT algorithm. Dimension (cm): 158: 96-101. https://doi.org/10.22213/2413-1172-2021-1-96-101
[15] Belkaid, A., Gaubert, J.P., Gherbi, A. (2016). An improved sliding mode control for maximum power point tracking in photovoltaic systems. Journal of Control Engineering and Applied Informatics, 18(1): 86-94.
[16] Kchaou, A., Naamane, A., Koubaa, Y., M'sirdi, N. (2017). Second order sliding mode-based MPPT control for photovoltaic applications. Solar Energy, 155: 758-769. https://doi.org/10.1016/j.solener.2017.07.007
[17] Kayisli, K. (2023). Super twisting sliding mode-type 2 fuzzy MPPT control of solar PV system with parameter optimization under variable irradiance conditions. Ain Shams Engineering Journal, 14(1): 101950. https://doi.org/10.1016/j.asej.2022.101950
[18] Bendib, B., Krim, F., Belmili, H., Almi, M.F., Bolouma, S. (2014). An intelligent MPPT approach based on neural-network voltage estimator and fuzzy controller, applied to a stand-alone PV system. In 2014 IEEE 23rd International Symposium on Industrial Electronics (ISIE), Istanbul, Turkey, pp. 404-409. https://doi.org/10.1109/ISIE.2014.6864647
[19] Shiau, J.K., Wei, Y.C., Chen, B.C. (2015). A study on the fuzzy-logic-based solar power MPPT algorithms using different fuzzy input variables. Algorithms, 8(2): 100-127. https://doi.org/10.3390/a8020100
[20] Gohar Ali, H., Vilanova Arbos, R., Herrera, J., Tobón, A., Peláez-Restrepo, J. (2020). Non-linear sliding mode controller for photovoltaic panels with maximum power point tracking. Processes, 8(1): 108. https://doi.org/10.3390/pr8010108
[21] Hameed, A., Zad, H.S., Ulasyar, A., Hashim, J. (2020). Robust sliding mode control based maximum power point tracking of solar photovoltaic system. In 2020 3rd International Conference on Computing, Mathematics and Engineering Technologies (iCoMET), Sukkur, Pakistan, pp. 1-6. https://doi.org/10.1109/iCoMET48670.2020.9073886
[22] Chiu, C.S., Ouyang, Y.L., Ku, C.Y. (2012). Terminal sliding mode control for maximum power point tracking of photovoltaic power generation systems. Solar Energy, 86(10): 2986-2995. https://doi.org/10.1016/j.solener.2012.07.008
[23] Mostafa, M.R., Saad, N.H., El-sattar, A.A. (2020). Tracking the maximum power point of PV array by sliding mode control method. Ain Shams Engineering Journal, 11(1): 119-131. https://doi.org/10.1016/j.asej.2019.09.003
[24] Ali, H.G., Vilanova, R., Pelez-Restrepo, J. (2020). Perturb & observe based adaptive sliding mode MPPT control of solar photovoltaic system. In 2020 IEEE International Conference on Environment and Electrical Engineering and 2020 IEEE Industrial and Commercial Power Systems Europe (EEEIC/I&CPS Europe), Madrid, Spain, pp. 1-6. https://doi.org/10.1109/EEEIC/ICPSEurope49358.2020.9160539
[25] Azzouzi, M. (2013). Optimization of photovoltaic generator by using PO algorithm under different weather conditions. Journal of Control Engineering and Applied Informatics, 15(2): 12-19.
[26] Besheer, A.H., Kassem, A.M., Abdelaziz, A.Y. (2014). Single-diode model based photovoltaic module: Analysis and comparison approach. Electric Power Components and Systems, 42(12): 1289-1300. https://doi.org/10.1080/15325008.2014.927024
[27] Petcut, F.M., Leonida-Dragomir, T. (2010). Solar cell parameter identification using genetic algorithms. Journal of Control Engineering and Applied Informatics, 12(1): 30-37.
[28] Dragomir, T.L., Petreuş, D.M., Petcuţ, F.M., Ciocan, I.C. (2010). Comparative analysis of identification methods of the photovoltaic panel characteristics. In 2010 IEEE International Conference on Automation, Quality and Testing, Robotics (AQTR), Cluj-Napoca, Romania, pp. 1-6. https://doi.org/10.1109/AQTR.2010.5520674
[29] Yu, G.J., Jung, Y.S., Choi, J.Y., Kim, G.S. (2004). A novel two-mode MPPT control algorithm based on comparative study of existing algorithms. Solar Energy, 76(4): 455-463. https://doi.org/10.1016/j.solener.2003.08.038
[30] Liu, J. (2018). Intelligent Control Design and MATLAB Simulation. Singapore: Springer.

NOMENCLATURE

I_{pv}	current output from the PV array, A
V_{pv}	voltage output from the PV array, V
P_{pv}	power output from the PV array, W
N_s	total count of solar panels wired in series
N_p	total count of solar panels connected in parallel
R_s	series resistor, Ω
R_p	parallel resistor, Ω
I_o	system output current, A
V_o	system output voltage, V
P_o	system output power, W
G	intensity of solar radiation, W/m^2
T	temperature of the PV system, ºC
I_L	the induced current
R_o	the circuit load, Ω
U	the pulse width
L	inductor, H
$\bar{L}$	uncertain parameters of inductor, H
C_v	input capacitor, F
C_o	output capacitor, F
$\bar{C}_v$	uncertain parameters of capacitors, F
V_{ref}	the reference voltage, V
e_1	reference voltage tracking error, V

Greek symbols

δ	the ideality factor
ζ	system state variable
ψ	uncertain parameters and external disturbances
κ_1	coefficient of a sliding surface
κ_2	switching factor of a sliding mode controller
ξ	update factor

Subscripts

ref	reference
L	induced
s	series
p	parallel
o	output
pv	photovoltaic